AN ANALYSIS ON THE RELIABILITY OF A SERIES OF TEXTURE AND SHAPE DESCRIPTORS FOR MELANOMA DIAGNOSIS

Andreea UDREA[1], Dumitru POPESCU[2], Cristian MIRON[3]

Early detection of melanoma can substantially reduce the mortality rate associated to this aggressive type of skin cancer. In this paper, a series of second order statistics texture descriptors are investigated for relevance in (normalised) RGB, HSV, YCrCb CIEXYZ and CIELab color spaces, along with a series of shape features. The best results are obtained for the following shape descriptors: contour asymmetry index, circularity index and mass-radius fractal dimension and for the following texture descriptors: uniformity for the RGB channels. These can be used along with other skin lesions descriptors for a high accuracy automated classification algorithm for melanoma early detection.

Keywords: conventional images analysis, melanoma diagnosis, second order statistics texture descriptors, shape descriptors

1. Introduction

Skin cancer is one of the most common malignancies in populations with fair skin. The incidence of skin cancer increases significantly from year to year [1]. This can be translated into increased number of deaths and larger treatment costs. There are two main classes of skin cancer: melanoma and non-melanoma cancer.

Melanoma is the most aggressive type of skin cancer, with a high associated morbidity and mortality rate. It is characterized by abnormal color and shape and rapid development, when compared to benign lesions.

In the last 10 years, the interest in analysing skin lesions, mainly using dermatoscopy images, in order to provide early melanoma diagnosis increased visibly due to the context presented above and subjectivity of dermatologists and general practitioners in delivering a diagnosis. (The gold standard in dermatology is the histopathological result, but it involves the lesion's excision.)

[1] Assoc. Prof., Dept. of Automatic Control and Systems Engineering, University POLITEHNICA of Bucharest, Romania, e-mail: andreea.udrea@acse.pub.ro

[2] Prof., Dept. of Automatic Control and Systems Engineering, University POLITEHNICA of Bucharest, Romania, e-mail: dumitru.popescu@acse.pub.ro

[3] PhD student, Dept. of Automatic Control and Systems Engineering, University POLITEHNICA of Bucharest, Romania

A series of other CAD (computer aided diagnosis) systems [2], [3] or semiautomatic diagnosis applications [4] were proposed in the literature. The steps generally taken in providing a diagnosis are: preprocessing (filters for noise and artifacts removal); contour extraction; shape, texture, color descriptors identification and selection; and classification using these descriptors. The analyzed images are dermatoscopic images which provide submacroscopic details of the analysed lesions.

The methods employed at each step vary from one study to the other [5], but, overall, the procedure mimics the ABCDE method which quantifies the asymmetry, border, color, diameter and elevation of a lesion. This method is not necessarily the most effective in providing an accurate diagnosis.

The most popular boundary extraction methods are as described in [6], while methods with superior results can be found in [7], [8], [9]. Each method leads to different outcomes, depending on the type of lesion of interest and image type.

The lesion descriptors refer to the color, texture and contour properties of the analyzed lesion [10], [11], [12].

The classification procedures broadly vary from study to study [13]. The sensibility and specificity of each application varies function of selected descriptors, classification method, images types and image database size and content.

In parallel to the development of these applications, the advances in technology facilitate the public use of powerful image acquisition devices like (smartphone) cameras. Mobile applications that acquire images of skin lesions and provide a diagnosis have been created. The medical world feedback regarding e-health and m-health applications dedicated to laypersons for melanoma diagnosis is controversial [14], [15].

In this context, we are implementing and constantly perfecting a medical app that offers a degree of risk associated to pigmented nevi [16]. It was tested for accuracy in a clinical trial and the conclusion was that it detects melanoma with a sensibility of 73% and has a specificity of 83%. The algorithm for skin lesions risk assessment uses local fractal analysis and classical image analysis; for lesions classification a rule-based algorithm is used. This was the first study that tests the accuracy of an app in detecting melanoma.

Following the study conclusions, we have investigated potential methods to produce other trustworthy descriptors for skin lesions when using a smartphone camera to acquire images. In [17] we present a preliminary study on a series of texture and shape related skin descriptors, obtaining satisfactory results. In this paper we present our latest results, on a larger database and considering an extended set of texture and shape features. The image analysis methods are detailed in section 2 and the results are presented and discussed in chapter 3.

2. Materials and methods

2.1. Conventional image acquisition and pre-processing

One of the common problems of conventional (non-medical) images taken with cameras/smartphone cameras is that the acquisition conditions may vary (different light sources, non-homogenous illumination, different distances and angles) and this can reflect in the diagnosis results. Other problems that can appear are that, besides the lesion of interest, other elements can be captured (other lesions, marks or objects); the lesion of interest is not completely captured; the focused degree is low. In other words, one does not deal with standardized medical images.

In order to obtain high quality images for analysis, we are using an app designed specifically for this task [17]. The lesions are also guaranteed to be completely imaged and centred (Fig.1.a), the images are focused and shadows free.

For this study, 480 images were acquired: 342 contain benign lesions and 138 melanomas. The lesions' type is confirmed by the histopathological results.

The image pre-processing steps consist in transforming the color image in a grey scale image and applying a median filter.


a)

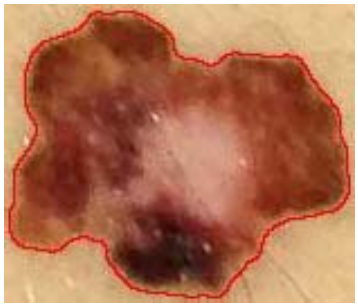
b)

Fig.1. a) Conventional skin lesion image b) Extracted region of interest

The next step is calculating the image histogram and identifying the threshold that best separates the lesion from the image. For this, the Otsu method is used. The grey level image is transformed into a binary image by applying the identified threshold. All the distinct, connected sets are identified and the largest set is considered to be the region (lesion) of interest and it is extracted from the image (Fig.1.b)). The lesion's area - A, perimeter - P, centre - (x_c,y_c), vector containing the lengths of the radii- r and the largest diameter - D_{max} are determined. These will be used for shape descriptors computation.

2.2. Texture descriptors

For each lesion, the texture information is analysed in a series of color spaces: RGB, normalised RGB, HSV, YCbCr, CIELab and CIEXYZ. The grey scale representation of the color image is also investigated.

In each color space (for each color channel) and, respectively, for the grey scale image, the normalised co-occurrence matrixes – *CM* – is computed. *CM* gives the distribution of co-occurring pixels values. Let *I* be the matrix of values of an image channel. *CM* has the general formula [18]:

$$CM(l_x, l_y) = \frac{1}{N}\sum_{i=1}^{W}\sum_{j=1}^{H}\begin{cases}1, & if \;\; I(i,j) = l_x \;\; and \;\; I(i+d_i, j+d_j) = l_y \\ 0, & otherwise\end{cases} \tag{1}$$

where: N is the number of co-occurrence pairs (used for normalization), d_i and d_j – the distances between the position of the analysed values and l_x and l_y, the values levels. Considering a grey scale image, if one considers 256 levels of grey, a 256x256 *CM* matrix is obtained. If a lower dimension matrix is desired, one can reduce the number of quantization/values levels l of the analysed image channel. For example, if l is reduced to 64, the *CM* size is 64×64. The effects of using different quantization levels is analysed in the next section. For this study, the considered distance in between co-occurring values is 1 (pairs of neighbour pixels are investigated).

CM is sensitive to rotations, so in order to obtain a degree of rotational invariance, *CM* for the horizontal (0^o), vertical (90^o) and diagonal directions (-45^o and -135^o) are investigated and the mean value of these 4 matrixes is used for further analysis.

In order to characterize the texture using *CM*, the following second order statistical parameters were computed: the contrast/variance (0 for constant channel values), correlation (1 perfectly correlated values, -1 negatively correlated value, not a number for constant channel values), energy/uniformity (1 for constant channel values) and homogeneity (1 for diagonal *CM*, gives the closeness of elements distribution to *CM* diagonal, range [0,1]) . They are given by expression (2), (3), (4) and, respectively, (5):

$$Cn = \sum_{i=1}^{l}\sum_{j=1}^{l}|i-j|^2 \, CM(i,j) \tag{2}$$

$$Cr = \sum_{i=1}^{l}\sum_{j=1}^{l}\frac{(i-\mu_i)(j-\mu_j)CM(i,j)}{\sigma_i\sigma_j} \tag{3}$$

where:

$$\mu_i = \sum_{i=1}^{l} i \sum_{j=1}^{l} CM(\mathrm{i,j}); \quad \mu_j = \sum_{j=1}^{l} j \sum_{i=1}^{l} CM(\mathrm{i,j})$$

$$\sigma_i^2 = \sum_{i=1}^{l} (\sum_{j=1}^{l} CM(\mathrm{i,j}) - \mu_i(i))^2; \quad \sigma_j^2 = \sum_{j=1}^{l} (\sum_{i=1}^{l} CM(\mathrm{i,j}) - \mu_j(j))^2$$

$$Un = \sum_{i=1}^{l} \sum_{j=1}^{l} CM(\mathrm{i,j})^2 \tag{4}$$

$$Hm = \sum_{i=1}^{l} \sum_{j=1}^{l} \frac{CM(\mathrm{i,j})}{1+|i-j|} \tag{5}$$

Also, the entropy of each image channel is calculated using the formula:

$$En = \sum_{i=1}^{W} \sum_{j=1}^{H} I(\mathrm{i,j}) \log(\mathrm{I(i,j)}) \tag{6}$$

These measures are usually investigated on the grey levels co-occurrence matrix. To the present, there are a lot of studies, each favouring a specific color space for lesion analysis. In this study, the texture is investigated in different color spaces and the results are compared in order to find the one that gives the most reliable texture descriptors.

2.3. Shape descriptors

In this section the shape descriptors considered for this study are briefly presented. First of all, a series of classical shape descriptors: the circularity index, the perimeter-area ratio, the perimeter-largest diameter ratio are investigated, than an asymmetry index and two fractal dimension estimation methods are proposed for contour irregularity characterisation.

The circularity index – i_{ci} - estimates how close an object's shape is to a perfect circle. For a circle i_{ci} equals 1, otherwise is greater than 1. It is calculated by using the following formula:

$$i_{ci} = \left(\frac{4\pi A}{P^2} \right)^{-1} \tag{7}$$

The perimeter – area ratio index - i_{pa} - is given by relation (8):

$$i_{pa} = \frac{P}{A} \tag{8}$$

The perimeter – largest diameter ratio index- i_{pd}- is calculated using the next expression:

$$i_{pd} = \frac{P}{D_{\max}} \tag{9}$$

The contour asymmetry index - i_{ca} is computed as follows:

$$i_{ca} = \frac{\min\left(\sum_{i=k}^{k+[P/2]} (r[i] - r[j])^2\right)}{A}, k = 1,[P/2]; \qquad j = \begin{cases} i+[P/2], i+[P/2] \le P \\ i+[P/2]-P+1, i+[P/2] > P \end{cases} \tag{10}$$

If the object is perfectly symmetrical with respect to one axes then i_{ca} equals 0, otherwise i_{ca} is larger than 0.

The fractal dimension of a contour gives a measure of the analysed boundary irregularity (how the observed object covers the space). There are several methods to estimate the fractal dimension; in this paper two are used for skin lesion boundary characterization: the box-counting method and the mass-radius method.

The standard Box-Counting method [19] determines the fractal dimension -d_f – by successive coverages of the image containing C with grids of squares of equal sides r_k. For each coverage, the squares that contain a part of the analysed contour are counted– N_k (r_k). The formula for d_f is:

$$df = \lim_{k \to \infty} \frac{\log(N_k)}{\log(1/r_k)} \tag{11}$$

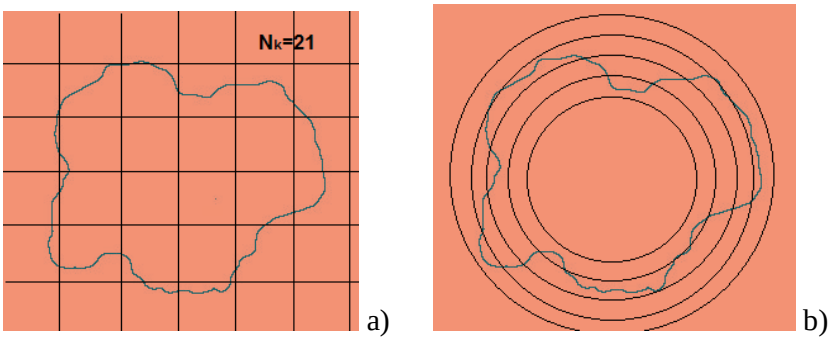

a) b)

Fig.2 a) Box-counting coverage; b) Mass- radius coverage

The points of coordinates $(\log(N_k\ (r_k)),\ \log(1/\ r_k))$ are approximately positioned in a line and its slope is the fractal dimension in "box-counting" sense. For the numerical implementation r_k takes values that are powers of 2. If the measured object is a straight line, d_f is 1, while if it covers the whole space d_f is 2.

The Mass-radius method [20] uses concentric circles for coverage. The mass-radius fractal dimension - d_{mr} - estimation formula is give bellow:

$$d_{mr} = \lim_{r_k \to 0} \frac{\log(A_{r_k})}{\log(r_k)} \tag{12}$$

where: A_{rk} is the sum of all pixels in C that are inside the circle of radius r_k, centred in (x_c,y_c). For the numerical implementation, r_k varies in between the smallest and largest radius.

3. Statistical results and discussion

In order to investigate the proposed descriptors' relevance, 480 images (342 normal nevi and 138 of melanomas) have been used. They were divided into a training set and a test set (equal number of melanomas and normal lesion/ set).

All images were subjected to the pre-processing steps described in section 2.1. The texture descriptors presented in 2.2 were calculated for the grey scale image and for each color channel of each the color model, for 3 quantization levels: channel's values range, channel's values range divided by 2 and, respectively, divided by 4. For each image we have 95 texture descriptors. The 6 shape descriptors for each lesion are calculated using the formulas in section 2.3.

A descriptor is considered relevant if the sensitivity (*Ss*) and specificity (*Sp*) of the classification are high enough:

$$Ss = \frac{TP}{TP+FN}\cdot 100 \quad Sp = \frac{TN}{TN+FP}\cdot 100$$
$$Ac = \frac{TN+TP}{TN+FP+TP+FN}\cdot 100 \tag{13}$$

where: *Ac*- stands for accuracy, *TP* (true positive) stands for the number of melanomas correctly identified, *FN* (false negative) is the number of melanomas that are not is correctly identified, *TN* (true negative) is the number of benign lesion that are correctly identified and *FP* (false positive) the number of benign lesions that are not correctly identified as normal.

A descriptor is considered to be potentially relevant for melanoma detection if it classifies the lesions in the training set with specificity (Sp_{tr}) higher

than 80%. Considering this condition, the values (V) that best separates the lesions in benign and melanoma are determined and the sensitivity (Ss_{tr}) and specificity (Sp_{tr}) are calculated on the training set. Using V, the specificity (Sp_{test}) and sensitivity (Se_{test}) are calculated on the test set. If the descriptor's value for a lesion is larger than V (i_{ci}, i_{pa}, i_{pd}, i_{ca}, d_f, d_{mr}, *En*, *Cn*), respectively, lower than V (|*Cr*|, *Un*, *Hm*) , we consider that this is an indication for melanoma. The obtained results can be found in Table 1– for texture descriptors and Table 2 – for shape descriptors. The table entrances marked with "-" stand for predictors with $Sp_{tr}<80\%$.

Table I

Texture descriptors: sensitivities and specificities values obtained on the test set

CM Level		Channel values range			Channel values range/2			Channel values range/4		
Channel	Descriptor	**Ss_{test} [%]**	**Sp_{test} [%]**	**V**	**Ss_{test} [%]**	**Sp_{test} [%]**	**V**	**Ss_{test} [%]**	**Sp_{test} [%]**	**V**
Grey level image	En	11.59	85.96	6.17	11.59	85.96	6.17	13.2	79.53	6.17
	Cn	1.44	76.6	521.42	1.44	76.60	78.60	14.4	79.53	19.39
	Cr	**53.62**	**83.04**	0.97	**53.62**	**83.04**	0.97	37.6	86.55	0.97
	Un	**47.82**	**79.53**	0.09	**49.27**	**78.36**	0.09	**50.7**	**83.04**	0.10
	Hm	47.82	70.76	0.53	47.82	71.34	0.66	40.5	81.29	0.76
Red channel	En	18.84	88.30	6.07	18.84	88.30	6.07	23.1	79.53	6.07
	Cn	0	80.11	476.40	0	80.11	72.0	3.04	79.53	17.70
	Cr	33.33	91.22	0.98	33.33	91.22	0.98	37.68	90.06	0.97
	Un	**46.37**	**79.53**	0.10	**47.82**	**78.94**	0.10	**56.52**	**81.29**	0.10
	Hm	46.37	71.92	0.53	46.37	71.34	0.66	36.23	79.53	0.76
Green channel	En	-	-	-	-	-	-	-	-	-
	Cn	1.44	75.43	529.25	1.44	75.43	79.88	14.49	79.53	19.65
	Cr	**53.62**	**82.45**	0.97	**53.62**	**82.45**	0.97	36.23	86.55	0.97
	Un	**47.82**	**80.11**	0.09	**49.27**	**77.77**	0.09	**56.52**	**79.53**	0.09
	Hm	49.27	71.92	0.5255	50.72	70.1	0.6	40.58	81.87	0.76
Blue channel	En	8.69	87.71	6.1940	8.69	87.7	6.19	10.14	81.29	6.19
	Cn	1.44	76.02	563.99	1.44	76.02	84.95	14.49	79.53	20.94
	Cr	21.73	94.15	0.98	21.73	94.15	0.98	18.84	92.98	0.98
	Un	**46.37**	**80.70**	0.08	**47.81**	**79.53**	0.08	**56.52**	**79.53**	0.09
	Hm	50.72	73.09	0.51	49.27	72.51	0.65	39.13	83.04	0.75
Hue channel	En	14.49	86.54	5.13	14.49	86.54	5.13	30.43	80.12	5.13
	Cn	-	-	-	-	-	-	-	-	-
	Cr	-	-	-	-	-	-	-	-	-
	Un	-	-	-	-	-	-	-	-	-
	Hm	-	-	-	-	-	-	-	-	-
Saturation channel	En	11.59	84.79	6.40	11.59	84.79	6.40	21.74	80.12	6.40
	Cn	-	-	-	-	-	-	-	-	-
	Cr	-	-	-	-	-	-	-	-	-
	Un	-	-	-	-	-	-	-	-	-
	Hm	-	-	-	-	-	-	-	-	-
Value channel	En	18.84	87.71	5.87	18.84	87.71	5.87	17.39	80.12	5.8
	Cn	-	-	-	-	-	-	-	-	-
	Cr	-	-	-	-	-	-	-	-	-
	Un	-	-	-	-	-	-	-	-	-
	Hm	-	-	-	-	-	-	-	-	-
Y channel	En	-	-	-	-	-	-	-	-	-
	Cn	-	-	-	-	-	-	-	-	-
	Cr	**55.07**	**82.45**	0.97	**56.52**	**82.45**	0.97	40.58	84.21	0.97
	Un	**47.82**	**76.02**	0.05	**47.82**	**77.77**	0.06	**53.62**	**80.12**	0.08
	Hm	47.82	71.92	0.48	52.17	70.76	0.61	49.28	79.53	0.72

Cb channel	En	17.39	76.60	3.73	17.39	76.60	3.73	27.5	81.29	3.7
	Cn	20.28	75.43	2.11	21.73	78.36	0.39	15.9	79.53	0.15
	Cr	-	-	-	14.49	85.38	0.98	18.8	88.30	0.97
	Un	40.57	78.36	0.13	46.37	72.51	0.19	26.0	80.12	0.35
	Hm	40.57	75.43	0.85	33.33	76.02	0.92	15.9	83.04	0.96
Cr Channel	En	31.88	73.09	3.86	31.88	73.09	3.86	**53.6**	**79.53**	3.86
	Cn	34.78	74.26	2.98	33.33	75.43	0.50	36.2	82.46	0.19
	Cr	-	-	-	-	-	-	15.9	87.72	0.98
	Un	40.57	73.68	0.12	27.53	77.19	0.18	17.3	80.12	0.29
	Hm	43.47	67.25	0.83	30.43	76.60	0.91	10.1	85.3	0.95

Table 2

Shape descriptors: sensitivities and specificities values obtained on the test set

Shape descriptor	**Ss_{test} [%]**	**Sp_{test} [%]**	**V**
Contour asymmetry index	**66.67**	**78.36**	2.52
Perimeter – area ratio index	33.33	72.51	0.073
Perimeter- largest diameter ratio index	5.13	87.72	4.71
Circularity index	**63.77**	**82.46**	1.26
Contour's fractal dimension (Box-counting method)	49.37	76.02	1.15
Contour's fractal dimension (Mass-radius method)	**60.87**	**79.53**	2.34

Discussion on the texture descriptors:

1. It can be observed that the overall best results for the texture descriptors are obtained for the RGB color model and the grey scale image.
2. The poorest results are obtained for CIELab, normalised RGB and CIEXYZ (in their cases we have not obtained $Sp_{tr}>80\%$ and the results are not included in Table I.).
3. The image's/cannel's uniformity is the best predictor – with a standalone accuracy of around 70% for most of the color channels and quantification levels.
4. The best results are achieved for the smallest quantisation level considered in this study ($l=4$). By the choice of a smaller value for the quantization levels the accuracy dropped (the results were not included in Table I.)

Discussion on the shape descriptors:

1. The best results for the shape descriptors were obtained by the contour asymmetry index, the circularity index and the fractal dimension estimated with the mass-radius method.

2. The main problem in the case of shape descriptors is the border extraction algorithm performance. In 5% of the cases, the proposed method leads to erroneous contours (mainly in case of light color, less pigmented lesions). In the future we are going to develop and test for performances other methods for lesion contour extraction.

3. The considered shape descriptors seem more reliable than the classical texture descriptors chosen for this study. This class of texture descriptors may be a solution in case of dermatoscopies, where the textural details: submacroscopic morphologic structures and vascular patterns that are located at different skin layers are clearly visible.

The results obtained in this study are consistent with the preliminary results obtained in [17] on a smaller database.

Compared to the overall performances obtained in [16] on the same proprietary database, the identified reliable descriptors have promising sensibility and specificity, especially the shape descriptors. Their standalone performances vary from the point of view of sensibility between 60% and 67% (while the specificity is around 80%) while in the case presented in [16], where 6 descriptors were used for classification, the sensibility was 73% and the specificity 83%.

For the improvement of the automatic classification algorithm that we develop we will consider for texture descriptors the *CM* uniformity for the red, green and blue channels of the RGB model and, also, of the grey scale image and, for shape descriptors: the contour asymmetry index, the circularity index and the fractal dimension estimated with the mass-radius method. These can be incorporated along the existent descriptors presented in [16].

Machine learning algorithms: support vector machines (SVM) and K nearest neighbor (KNN) are to be tested for performances in the context of the classification procedure.

4. Conclusions

Creating a reliable early melanoma diagnosis m-health application is feasible. Introducing an elevated number of reliable descriptors is of paramount importance. With this study we conclude that the RGB color space and the grey scale representation of the image give the best results for second order statistics textural descriptors (mainly uniformity) and that the proposed contour asymmetry index, the circularity index and the fractal dimension estimated with the mass-radius method are reliable shape descriptors.

Increasing the image database, using the identified features along with other color, texture and shape parameters and using machine learning algorithm

for classification can lead to a high accuracy early melanoma diagnosis app for laypersons.

Acknowledgement

The work of Andreea Udrea was supported by Project SOP HRD - PERFORM /159/1.5/S/138963.

R E F E R E N C E S

[1] *E. G. Little, M. J. Eide*, "Update on the current state of melanoma incidence", Dermatol Clin., vol.30, 2012, pp. 355-61

[2] *A. Safi, M.Baust, O. Pauly, V. Castaneda, T. Lasser, D. Mateus, N. Havab, R. Hein, M. Ziai*, "Computer–Aided Diagnosis of Pigmented Skin Dermoscopic Images Medical Content-Based Retrieval for Clinical Decision Support", Lecture Notes in Computer Science, vol. 7075, 2012, pp 105-115

[3] *W. Chang, A. Huang, C. Yang, C. Cjen, R. Wu, G. Chen*, "Computer-Aided Diagnosis of Skin Lesions Using Conventional Digital Photography: A Reliability and Feasibility Study", Plos ONE, vol.8, 2013

[4] *O. Razeghi, G. Qiu, H. Williams, K. Thomas*, "Computer Aided Skin Lesion Diagnosis with Humans in the Loop", Machine Learning in Medical Imaging, Lecture Notes in Computer Science Volume 7588, 2012, pp 266-274

[5] *J. Premaladha, S. Sujitha, M. Lakshmi Priya, K.S. Ravichandran*, "A Survey on Melanoma Diagnosis using Image Processing and Soft Computing Techniques", Research Journal of Information Technology, 6, 2014, pp. 65-80

[6] *M.E. Celebi, H. Iyatomi, G. Schaefer, W.V Stoecker*, "Lesion border detection in dermatoscopy images", Computerized Medical Imaging and Graphics 33(2), 2009, pp. 148-153

[7] *X. Li, B. Aldridge, L. Ballerini, R. Fisher, J. Rees*, "Depth data improves skin lesion segmentation", Proc. 12th Int. Conf. on Medical Image Computing and Computer Assisted Intervention (MICCAI), London, 2009, pp. 1100-1107

[8] *G. Schaefer, M. I.Rajab, M.E. Celebi, H., Iyatomi*, "Colour and contrast enhancement for improved skin lesion segmentation", Computerized Medical Imaging and Graphics 35(2), 2011, pp. 99 – 104

[9] *H. Wang, R. H.\ Moss, X. Chen, R.J. Stanley, W.V. Stoecker, M.E. Celebi, J.M. Malters, J.M. Grichnik, A.A. Marghoob, H.S. Rabinovitz, S.W. Menzies, T.M. Szalapski*, "Modified watershed technique and post-processing for segmentation of skin lesions in dermatoscopy images", Computerized Medical Imaging and Graphics 35(2), 2011, pp. 116- 120

[10] *T.K. Lee, E. Claridge*, "Predictive power of irregular border shapes for malignant melanomas", Skin Research and Technology 11(1), 2005, pp. 1-8

[11] *M. Mete, S. Kockara, K. Aydin*, "Fast density-based lesion detection in dermatoscopy images", Computerized Medical Imaging and Graphics 35(2), 2011, pp. 128- 136

[12] *W. Stoecker, M. Wronkiewiecz, R. Chowdhury, R.J. Stanley, J. Xu, A. Bangert, B. Shrestha, D.A. Calcara, H.S. Rabinovitz, M. Oliviero, F. Ahmed, L.A. Perry, R. Drugge*, "Detection of granularity in dermatoscopy images of malignant melanoma using color and texture features" *Computerized Medical Imaging and Graphics* 35(2), 2011, pp. 144 -147

[13] *I. Maglogiannis, C.N. Doukas*, "Overview of advanced computer vision systems for skin lesions characterization", *IEEE Transactions on Information Technology in Biomedicine* 13(5), 2009, pp. 721-733

[14] *Y. Robson, S. Blackford, D. Roberts*, "Caution in melanoma risk analysis with smartphone application technology", Br J Dermatol.,vol. 167, 2012, pp. 703-704
[15] *J.A. Wolf, J. K. Moreau, O. Akilov, et al*., "Diagnostic inaccuracy of smartphone applications for melanoma detection", JAMA Dermatol., vol. 149, 2013, pp. 422-426
[16] *T. Maier, D. Kulichova, K. Schotten, R. Astrid, T. Ruzicka, C. Berking, A. Udrea*, Accuracy of a smartphone application using fractal image analysis of pigmented moles compared to clinical diagnosis and histological result, Eur Acad Dermatol Venereol., vol. 29, iss.4, 2015, pp. 663-667
[17] *A. Udrea, C. Lupu,"* Real-time acquisition of quality verified non-standardized color images for skin lesions risk assessment – a preliminary study", Proceedings of 18th International Conference on System Theory, Control and Computing, Sinaia, 2014, pp. 199-204
[18] *R. M. Haralick, K. Shanmugam, I. Dinstein*, "Textural features for Image Classification", IEEE Transactions on Systems, Man and Cybernetics, Vol. 3, 1973, pp. 610-621
[19] *H.O. Peitgen, H. Jurgens, D. Saupe*, Chaos and Fractals: New Frontiers of Science, first ed, Springer, Berlin, 1992
[20] *G. Landini, J. W. Rippin*, "Notes on the implementation of the mass radius method of fractal dimension estimation", Computer Applications in the Biosciences, vol. 9, 1993, pp. 547–550.